

SCIENTIFIC REPORTS

OPEN

Preparation of a magnetic reduced-graphene oxide/tea waste composite for high-efficiency sorption of uranium

Aili Yang¹, Yukuan Zhu¹, Ping Li¹ & C. P. Huang²

The preparation and application of adsorptive materials with low cost and high-efficiency recovery of uranium from nuclear waste is necessary for the development of sustainable, clean energy resources and to avoid nuclear pollution. In this work, the capacity of tea waste and tea waste hybrids as inexpensive sorbents for uranium removal from water solutions was investigated. Composites of graphene oxide (GO) and tea waste (TW) exhibited a promising adsorption performance for uranium from aqueous solutions. The composites GOTW and magnetic rGO/Fe₃O₄/TW show high adsorption capacities ($Q_{m(TW)} = 91.72$ mg/g, $Q_{m(GOTW)} = 111.61$ mg/g and $Q_{m(rGO/Fe_3O_4/TW)} = 104.95$ mg/g) and removal rates (~99%) for U(VI). The equilibrium sorption of the adsorbents fitted well to the Langmuir model, and the sorption rate fitted well to a pseudo-second-order kinetic model. The thermodynamic parameters indicated that sorption was spontaneous and favourable. The prepared adsorbents were used for the removal of uranium from real water samples as well. The results revealed that GOTW and rGO/Fe₃O₄/TW can be used to remediate nuclear industrial effluent as a potential adsorbent.

To significantly reduce the emission of the greenhouse gas CO₂ from burning fossil fuels and avoid air pollution-related deaths, nuclear power from fission currently accounts for ~10% of the global electricity supply¹. Uranium is the main nuclear fuel of fission power reactors. However, uranium released into the environment and water results in serious hazards for various organisms, including humans, due to its high chemical toxicity, radioactivity and long half-life². The US Environmental Protection Agency has established a maximum contaminant level for uranium in drinking water to be 30 µg/L³. Consequently, researchers have investigated methods for the efficient removal and recovery of uranium from aqueous solutions to protect the environment and control nuclides pollution. At present, various methods have been developed to address uranium in water, including membrane separation^{4,5}, photoelectrochemical reduction⁶, biological treatment^{7,8}, solvent extraction^{9,10}, ion exchange^{11,12} and adsorption^{13–15}. Adsorption is the most extensively used approach for uranium removal because of its high efficiency, low cost, simple operation and low production of secondary pollution.

Different types of adsorbents have been successfully used for uranium removal from aqueous solutions, including natural polymers^{16,17}, inorganic compounds^{18,19}, carbon nanomaterials^{20,21}, metal-organic frameworks^{22,23} and biomass^{24,25}. The economy of the adsorbents used is of great importance to reduce wastewater treatment costs. Many researchers have focused on the removal of various pollutants by low-cost adsorbents derived from agricultural wastes^{26–28}. The re-utilization of agricultural wastes is increasingly becoming a significant concern due to their unique structures and outstanding physicochemical properties^{29,30}.

Tea has been the most widely consumed beverage in many countries due to its reported positive health benefits^{31,32}. The largest amount of production and consumption of tea is in China. The large amount of tea waste (TW) produced each year will inevitably result in severe environmental problems if not fully utilized. Tea leaves contain an abundance of active chemical constituents, including flavonoids, phenolic compounds, alkaloids and methylxanthines³³. Additionally, TW has several salient advantages such as being inexpensive, easy to handle and having wide availability³⁴. Therefore, it is necessary to take full advantage of TW to avoid environmental pollution and resource waste. TW has been widely investigated for the removal of various pollutants such as dyes³⁵,

¹Institute of Materials, China Academy of Engineering Physics, Jiangyou, 621907, China. ²Department of Environmental Engineering, University of Delaware, Newark, DE, 19716, USA. Correspondence and requests for materials should be addressed to A.Y. (email: yang770117@sina.com)

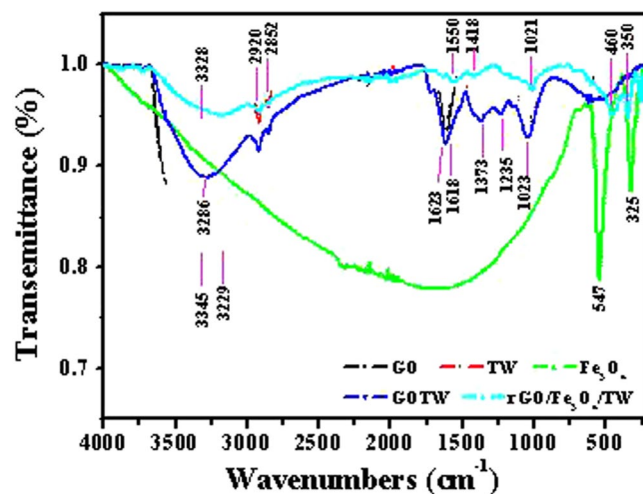


Figure 1. IR spectra of GO, Fe₃O₄, TW, GOTW and rGO/Fe₃O₄/TW.

oxytetracycline³⁶, ethylene³⁷, As and Ni³⁸, Cu³⁹, Cd⁴⁰, Pb⁴¹ and Hg⁰⁴². To the best of our knowledge, few studies have applied TW as an adsorbent for the adsorption of uranium from aqueous solutions^{43–46}, and the maximum sorption capacities (Q_m) for uranium loading by TW obtained in these reports are low (<150 mg/g). Moreover, there is no literature available on the adsorption of uranium onto a magnetic reduced graphene oxide/Fe₃O₄/TW (rGO/Fe₃O₄/TW) composite adsorbent.

At present, the development and applications of graphene and its derivatives have been hot research topics in various fields such as electronic devices, electrochemical capacitors, catalysts and environmental remediation, thanks to their unusual properties⁴⁷. Graphene oxide (GO) has been shown to be an excellent adsorbent for heavy metal ions (e.g., As⁴⁸, Eu⁴⁹, Cr⁵⁰, Pb⁵¹, Cu⁵² and U⁵³). GO has numerous active functional groups fixed on the surface including carboxyl, lactone, hydroxyl and phenolic hydroxyl⁵⁴. TW is rich in cellulose, whose hydroxyl groups can be combined with GO to form an ester linkage, introducing carboxyl groups to TW⁵⁵. In the present study, we prepared two novel composites, GOTW and rGO/Fe₃O₄/TW, and explored their application as an adsorbent for uranium(VI) from aqueous solutions. Moreover, the adsorptive performance for U(VI) was tested in a solution containing other cationic ions and in practical low-radioactive uranium-bearing nuclear wastewater. The results presented in this work reveal that the composite GOTW and magnetic rGO/Fe₃O₄/TW are promising adsorbents for the removal of uranium from nuclear industrial effluent.

Results and Discussion

Characterization of the products. The FT-IR spectra of GO, Fe₃O₄, TW, GOTW and rGO/Fe₃O₄/TW are shown in Fig. 1. The IR spectrum of GO was similar to that of GO in the reference⁵⁶ and had characteristic peaks at 3345–3229, 1725, 1618, 1387, 1227 and 1061 cm⁻¹, corresponding to the stretching vibrations of O-H, carbonyl and carboxyl C=O, aromatic C=C and H₂O, carboxyl O=C-O, and alkoxy C-O-C stretching vibrational modes, respectively. In the IR spectrum of TW, the broad peaks at 3328 cm⁻¹ could come from the -OH of absorbed H₂O (3200–3500 cm⁻¹) or N-H stretching. The double peaks at 2920 and 2852 cm⁻¹ were attributed to aliphatic carbons. The strong peaks at 1627 and 1026 cm⁻¹ indicated the carbonyl stretching of -COOH groups and stretching vibration of the C-O groups of polysaccharides, respectively. These characteristic peaks of the prepared TW were similar to that of tea wastes reported previously⁴³. However, compared to that of GO, double peaks at 2920 and 2852 cm⁻¹ attributed to aliphatic carbons appeared in the IR spectrum of GOTW, and the intensity of the characteristic peaks at 3286 cm⁻¹ ascribed to O-H was significantly lower, which suggests that the composite GOTW was prepared successfully. In the IR spectrum of rGO/Fe₃O₄/TW, there were characteristic peaks at 460 cm⁻¹ and 350 cm⁻¹ belonging to the Fe-O stretching vibration⁵⁷, and similar absorption peaks as TW, whereas the characteristic peaks assigned to the stretching vibrations of O-H, carbonyl and carboxyl C=O, aromatic C=C and H₂O, carboxyl O=C-O, and alkoxy C-O-C disappeared. Moreover, the stretching vibrations of C=C and epoxy C-O at 1550 and 1014 cm⁻¹ of rGO functional groups were present in the IR spectrum of rGO/Fe₃O₄/TW⁵⁸. These results implied that GO is reduced to rGO and that, simultaneously, Fe(II) is oxidized to Fe(III). The results showed that the magnetic composite rGO/Fe₃O₄/TW was prepared successfully.

The XRD patterns of the crystal phase of the prepared GO (a), Fe₃O₄ (b), rGO/Fe₃O₄/TW (c), GOTW (d) and TW (e) are presented in Fig. 2. No obvious diffraction peaks at $2\theta=10^\circ$ and 42° attributed to the crystal planes of GO were observed, confirming the reduction of GO to rGO. The XRD pattern of TW (Fig. 2e) was consistent with that previously reported for tea⁵⁹. Compared to those of GO and TW, differences in the peak intensities in the XRD pattern of GOTW (Fig. 2d) indicated that TW was successfully attached to the surface of GO. The XRD peaks at 2θ values of approximately 29.94° , 35.30° , 42.98° , 53.38° , 56.84° , 62.46° and 74.54° of the purchased Fe₃O₄ are shown in Fig. 2b. The diffraction peaks of the composite rGO/Fe₃O₄/TW (Fig. 2c) are consistent with those of Fe₃O₄, but the peak intensities were significantly lower with the addition of rGO and TW.

The morphologies of GO, TW and GOTW were observed by SEM. The morphology of rGO/Fe₃O₄/TW was analysed by AFM because of its magnetic properties. Figure 3a shows that GO exhibited a wrinkled lamellar

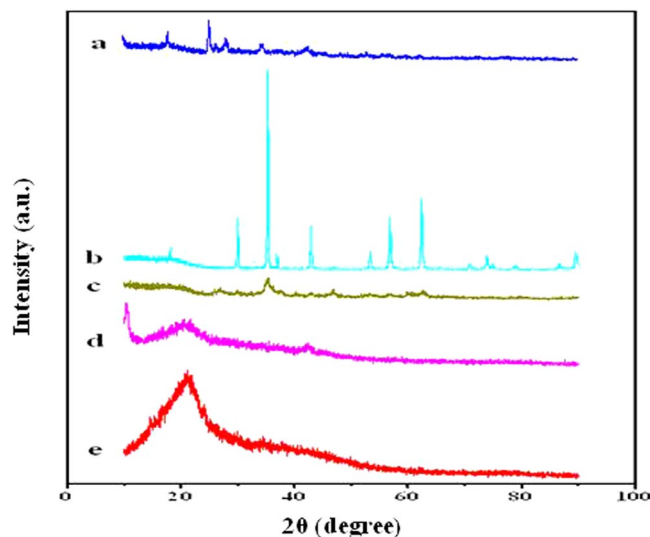


Figure 2. XRD patterns of GO (a), Fe_3O_4 (b), $\text{rGO}/\text{Fe}_3\text{O}_4/\text{TW}$ (c), GOTW (d) and TW (e).

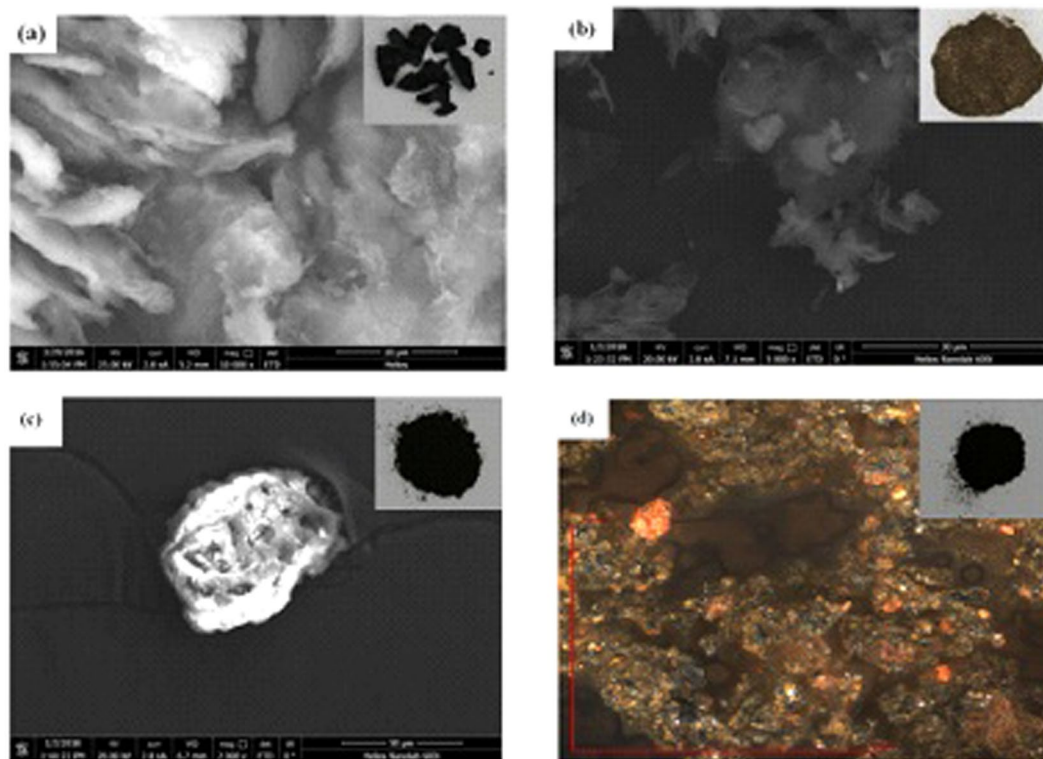


Figure 3. SEM images of GO (a), TW (b), GOTW (c) and AFM image of $\text{rGO}/\text{Fe}_3\text{O}_4/\text{TW}$ (d). Insets are optical digital photos of GO, TW, GOTW and $\text{rGO}/\text{Fe}_3\text{O}_4/\text{TW}$.

structure, and the sheets of GO stacked together due to strong inter-planar interactions. As shown in Fig. 3b, an irregular layered structure with a smooth surface without pores was observed in the SEM image of TW. However, the surface of GOTW (Fig. 3c) presented many tiny pores which could be propitious to adsorb heavy metal ions⁶⁰. In the AFM image of $\text{rGO}/\text{Fe}_3\text{O}_4/\text{TW}$ (Fig. 3d) we observed that many Fe_3O_4 particles were attached to the surface of GOTW. Moreover, as seen in the insets of Fig. 3, a significant difference in the macroscopic morphology of the prepared sorbents was observed.

Magnetic analysis of Fe_3O_4 and $\text{rGO}/\text{Fe}_3\text{O}_4/\text{TW}$ using a vibrating sample magnetometer (VSM) is shown in Fig. 4. The magnetization saturation values for Fe_3O_4 and $\text{rGO}/\text{Fe}_3\text{O}_4/\text{TW}$ were 100 and 10 emu/g, respectively. A nonlinear, reversible magnetization curve with no hysteresis exhibited characteristic super-paramagnetic behaviour. The reduced saturation magnetization was mainly due to the presence of diamagnetic GOTW surrounding

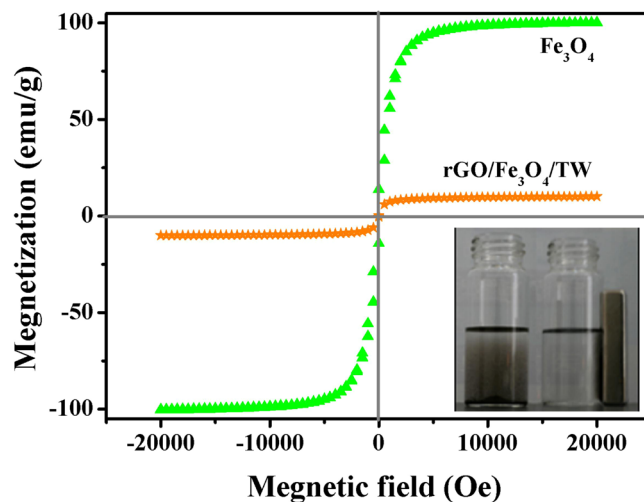


Figure 4. Magnetization curve of Fe_3O_4 and $\text{rGO}/\text{Fe}_3\text{O}_4/\text{TW}$. Inset is the separation application from the solution of $\text{rGO}/\text{Fe}_3\text{O}_4/\text{TW}$ by an external magnetic field.

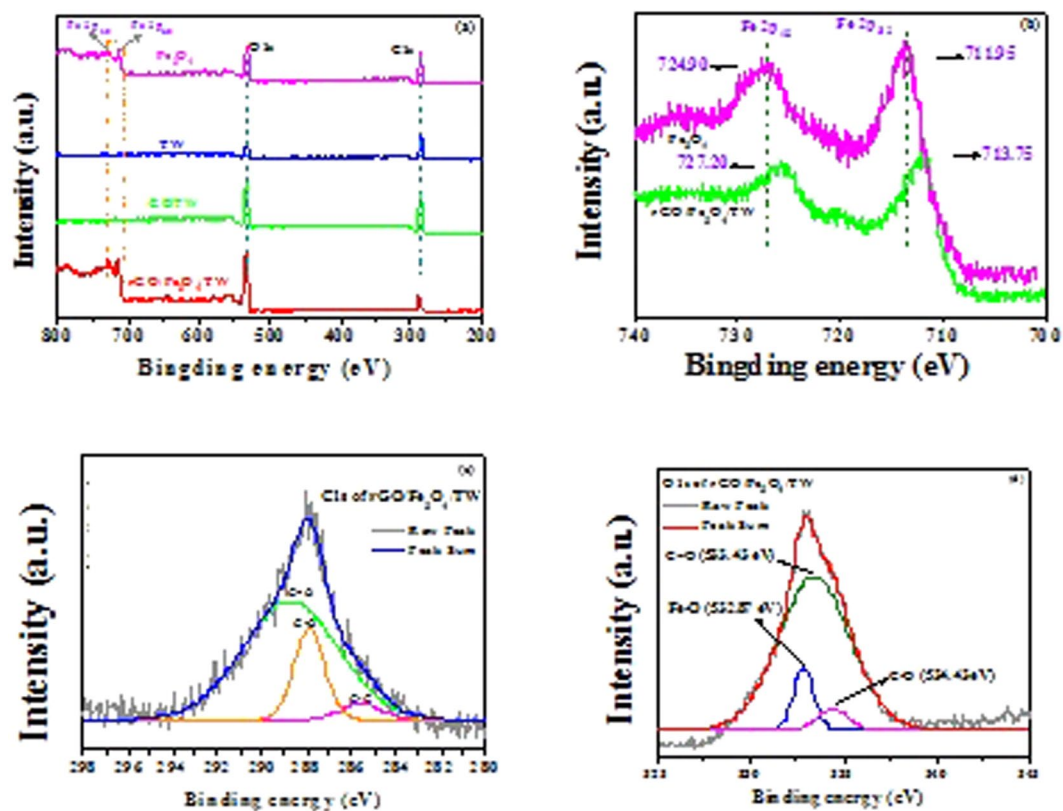


Figure 5. XPS survey spectra of Fe_3O_4 , TW, GOTW and $\text{rGO}/\text{Fe}_3\text{O}_4/\text{TW}$ (a), the high-resolution Fe 2p spectra of Fe_3O_4 and $\text{rGO}/\text{Fe}_3\text{O}_4/\text{TW}$ (b), the high-resolution C1s spectra of TW and $\text{rGO}/\text{Fe}_3\text{O}_4/\text{TW}$ (c) and the high-resolution O1s spectra of $\text{rGO}/\text{Fe}_3\text{O}_4/\text{TW}$ and Fe_3O_4 (d).

the Fe_3O_4 cores. However, as seen in the inset of Fig. 4, the composite $\text{rGO}/\text{Fe}_3\text{O}_4/\text{TW}$ can be completely separated from the solution by a conventional magnet.

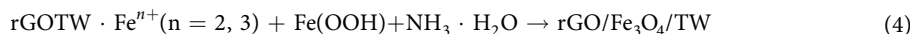
XPS analysis of the samples. The chemical composition of Fe_3O_4 , TW, GOTW and $\text{rGO}/\text{Fe}_3\text{O}_4/\text{TW}$ was investigated by XPS. The XPS survey spectra of $\text{rGO}/\text{Fe}_3\text{O}_4/\text{TW}$ (Fig. 5a) showed evident characteristic peaks at approximately 289, 557, 715 and 729 eV, which were attributed to C1s, O1s and Fe2p, respectively. In the high-resolution spectrum of Fe 2p (Fig. 5b), the peaks of $\text{Fe } 2p_{3/2}$ and $\text{Fe } 2p_{1/2}$ were located at 713.75 and 727.20 eV, respectively, indicating the presence of Fe_3O_4 in the composite $\text{rGO}/\text{Fe}_3\text{O}_4/\text{TW}$. The C1s and O1s

Peak	rGO/Fe ₃ O ₄ /TW		TW	
	Position/eV	%	Position/eV	%
C–C/C=C	285.60	4.07	284.99	78.53
C–O	287.88	18.76	286.81	2.93
C=O	288.74	77.17	287.27	18.54

Table 1. Curve fitting results of XPS C1s spectra of TW and rGO/Fe₃O₄/TW.

XPS peaks of TW and rGO/Fe₃O₄/TW were deconvoluted (Fig. 5c,d). Figure 5c shows the C1s spectra with three deconvoluted peaks at 283.8, 285.1 and 287.5 eV associated with C–C, C–O and C=O bonds, respectively. Figure 5(d) shows the O1s spectrum, and the three peaks at 529.6, 531.2 and 532.7 eV belong to Fe–O, C=O and C–O, respectively. The fit results are presented in Table 1. The oxygen-containing groups C–O and C=O were significantly more abundant after combination, implying that TW was successfully loaded onto the surface of GO.

Based on the results described above, a possible reaction mechanism for the composite rGO/Fe₃O₄/TW is illustrated in Fig. 6. First, GO combines with TW to form GOTW, and then Fe²⁺ ions react with GOTW by a redox reaction to form rGOTW as shown in Eq. (2) in which GO is as an oxidant. Because the hydrolysis of Fe³⁺ results in the formation of Fe(OOH), as shown in Eq. (3), the composite rGO/Fe₃O₄/TW was obtained after the addition of ammonia solution, as shown in Eq. (4).



Influence of pH on adsorption. The solution pH affects the speciation of uranium in solution and significantly influences the uranium adsorption process. The effect of pH on the adsorption of uranium (VI) by the synthesized adsorbents is presented in Fig. 7. The results showed a substantial impact of pH on uranium adsorption. The adsorption of U(VI) on TW, GOTW and rGO/Fe₃O₄/TW significantly increased with increasing pH from 2.0 to 5.0. At pH = 5, the removal rate of uranium of TW, GOTW and rGO/Fe₃O₄/TW reached the highest value. At pH < 4.0, uranium exists mainly in the form of UO₂²⁺. The competition between H₃O⁺ and UO₂²⁺ for binding sites on the adsorbent surface results in a low sorption efficiency⁶¹. At pH = 5.0–7.0, the prominent species of uranium in the solution are UO₂⁺, UO₂(OH)⁺, (UO₂)₂(OH)₂²⁺, (UO₂)₃(OH)₅⁺ and (UO₂)₄(OH)₇⁺⁶². As seen in Fig. 7, the removal rate of uranium significantly increases at pH > 5.0, which can be attributed to electrostatic interactions of these complex uranium ions with negatively charged groups on the surface of TW, GOTW and rGO/Fe₃O₄/TW. The sorption behaviour of UO₂²⁺ on GOTW and rGO/Fe₃O₄/TW at pH 2.0–7.0 is similar to that reported by Wang *et al.*¹³. Additionally, the sorption efficiency of uranium by GOTW and rGO/Fe₃O₄/TW was higher than that for TW, indicating that the composite of GO and TW had more efficient adsorption of uranium. Consequently, the optimum pH for U(VI) adsorption by TW, GOTW and rGO/Fe₃O₄/TW was 5.0.

Influence of contact time and kinetic study. The adsorption dynamics data^{63,64} were analysed based on Eqs (5) and (6). Figure 8(a) presents the time-dependent adsorption over a contact time ranging from 1 to 120 min of U(VI) by TW, GOTW and rGO/Fe₃O₄/TW. As seen in Fig. 8(a), the removal rate of the prepared adsorbents exceeded 96% within 1 min, and the adsorption equilibrium time was 60 min. Adsorption kinetic data of the pseudo-first-order and pseudo-second-order model at different temperature are given in Table 2. The correlation coefficient of pseudo-second-order model ($R^2 = 0.9999$ and 1.0000) was superior to the pseudo-first-order model, which indicated that the adsorption of U(VI) onto TW, GOTW and rGO/Fe₃O₄/TW fitted the pseudo-second-order model better. The fit results demonstrated that a chemical reaction played a significant role in the rate-controlling steps. The surface functional groups of the prepared adsorbents might form strong electrostatic and chemical interactions with U(VI) ions⁶⁵. Moreover, the kinetic model fits results and parameters of rGO/Fe₃O₄/TW at different temperature are shown in Fig. 8(b) and Table 2, respectively. The result shows that temperature has no evident effect on the adsorption rate of rGO/Fe₃O₄/TW.

$$\lg(Q_e - Q_t) = \lg Q_e - \frac{k_1}{2.303} t \quad (5)$$

$$\frac{t}{Q} = \frac{1}{k_2 Q_e^2} + \frac{t}{Q_e} \quad (6)$$

where k_1 (min⁻¹) is the Lagergren rate constant of adsorption, and k_2 (g/(mg·min)) is the rate constant of pseudo-second-order adsorption.

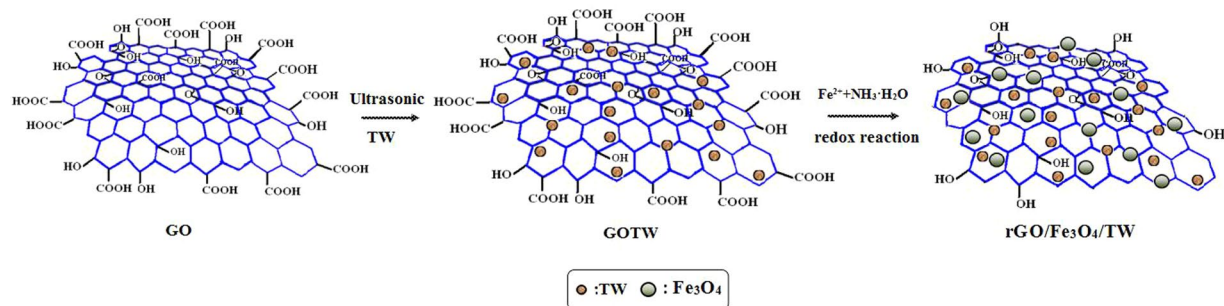


Figure 6. Schematic diagram of a possible formation mechanism of rGO/Fe₃O₄/TW.

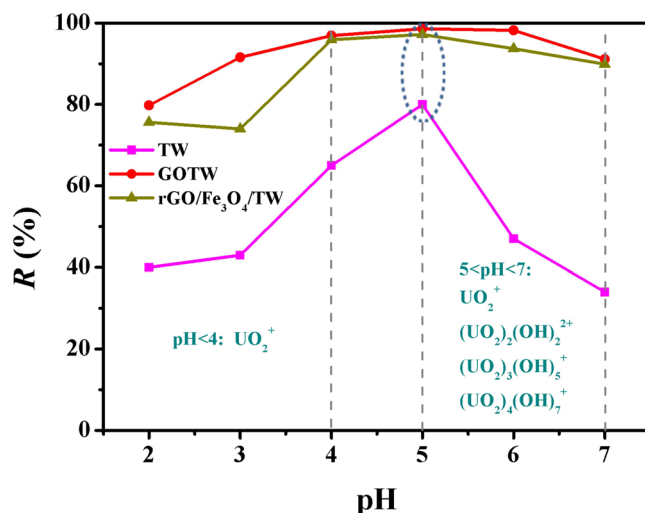


Figure 7. Effect of pH on the U(VI) adsorption by TW, GOTW and rGO/Fe₃O₄/TW. $C_{(\text{U})\text{initial}} = 10 \text{ mg/L}$, $C_{\text{adsorbent}} = 0.5 \text{ g/L}$, contact time = 30 min, and $T = 298 \text{ K}$.

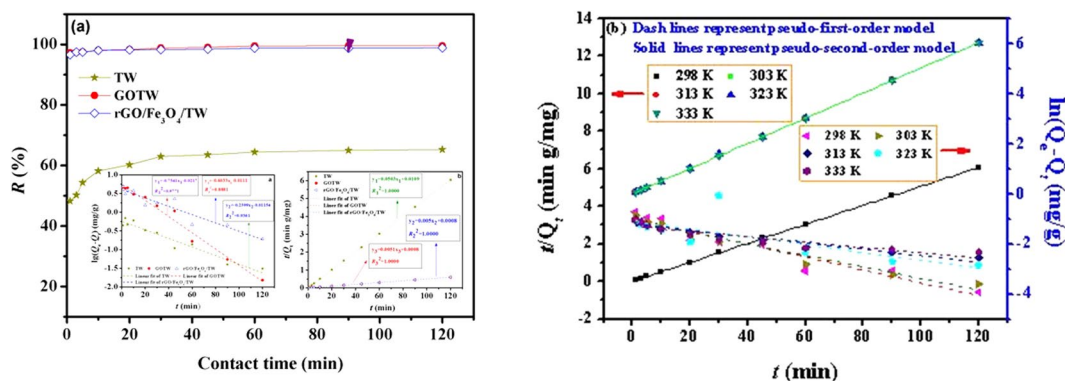


Figure 8. Influence of contact time on U(VI) sorption and kinetic fit of TW, GOTW and rGO/Fe₃O₄/TW at 298 K (a) and kinetic fit of rGO/Fe₃O₄/TW at different temperature (298 K–333 K) (b). $\text{pH} = 5.0$, $C_{(\text{U})\text{initial}} = 10 \text{ mg/L}$, $C_{\text{adsorbent}} = 0.5 \text{ g/L}$.

Adsorption isotherm. The Langmuir and Freundlich isotherm models are expressed in Eqs (7) and (8), respectively⁶⁶. The fit results of Langmuir and Freundlich isotherm models of GO, TW, GOTW and rGO/Fe₃O₄/TW at 298 K are shown in Fig. 9(a). The Langmuir and Freundlich isotherm models of rGO/Fe₃O₄/TW at different temperature are shown in Fig. 9(b). The isotherm parameters calculated from fitting processes at different temperature are listed in Table 3. The Langmuir equation of the adsorbents fitted the experimental data well, with a higher correlation coefficient (R^2).

Sorbents	Temperature (K)	Pseudo-first-order model			Pseudo-second-order model		
		Q_e (mg/g)	k_1 (min^{-1})	R^2	Q_e (mg/g)	k_2 (g/(mg·min))	R^2
TW	298	1.026	0.0002	0.7400	19.88	0.2321	1.0000
GOTW	298	5.677	0.0500	0.9796	20.00	0.3135	1.0000
rGO/Fe ₃ O ₄ /TW	298	0.104	0.0594	0.9328	19.80	0.3985	1.0000
	303	0.082	0.0530	0.9510	19.80	0.4305	1.0000
	313	0.061	0.0290	0.9335	19.84	0.5522	1.0000
	323	0.083	0.0364	0.5729	19.92	0.2083	0.9999
	333	0.051	0.0244	0.8482	19.92	0.7412	1.0000

Table 2. Parameters of pseudo-first-order and pseudo-second-order kinetic models for U adsorption by TW, GOTW and rGO/Fe₃O₄/TW at different temperature.

Sorbents	Temperature (K)	Langmuir model			Freundlich model			D-R model		
		Q_m (mg/g)	k_L (L/mg)	R^2	n	k_F ($\text{mg}^{1-n} \text{L}^n/\text{g}$)	R^2	Q_m (mg/g)	β (mol^2/J^2)	R^2
GO	298	79.108	0.3856	0.9901	2.89	26.3486	0.9134	59.369	10^{-7}	0.7866
TW	298	91.719	0.2151	0.9797	3.42	21.5161	0.9320	56.165	10^{-7}	0.9278
GOTW	298	111.614	0.4828	0.9682	3.84	38.4609	0.9006	78.830	10^{-8}	0.9277
rGO/Fe ₃ O ₄ /TW	298	103.840	0.7519	0.9892	4.07	40.2672	0.8838	72.341	5×10^{-8}	0.8664
	303	104.130	0.8218	0.9899	4.13	41.6600	0.8808	72.756	4×10^{-8}	0.8664
	313	107.210	0.8096	0.9912	4.17	42.7600	0.8887	73.821	4×10^{-8}	0.8632
	323	108.220	0.8689	0.9924	4.20	44.0200	0.8911	73.056	3×10^{-8}	0.8521
	333	109.160	0.9188	0.9934	4.27	45.2600	0.8899	73.831	3×10^{-8}	0.8557

Table 3. Langmuir, Freundlich and D-R model parameters for uranium adsorption on GO, TW, GOTW and rGO/Fe₃O₄/TW at different temperature.

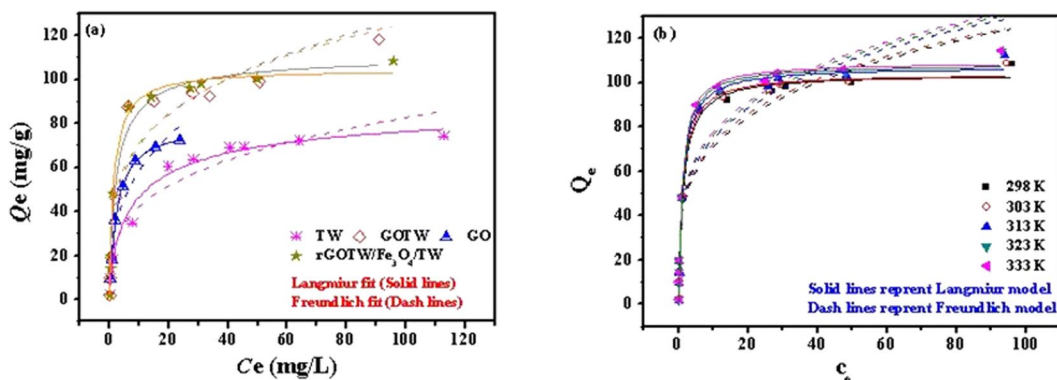


Figure 9. Langmuir and Freundlich isotherm models fit of GO, TW, GOTW and rGO/Fe₃O₄/TW at 298 K (a) and the isotherm models fit of rGO/Fe₃O₄/TW at different temperature (298 K–333 K) (b). pH = 5.0, $C_{(U) \text{ initial}} = 5\text{--}150$ mg/L, $C_{\text{sorbent}} = 0.5$ g/L, contact time = 24 h.

$$Q_e = \frac{Q_m \cdot K_L \cdot C_e}{1 + K_L C_e} \quad (7)$$

$$Q_e = K_F \cdot C_e^{1/n} \quad (8)$$

where Q_e (mg/g) is the equilibrium adsorption capacity, C_e (mg/L) is the uranium concentration at equilibrium, Q_m (mg/g) is the maximum adsorption capacity, K_L (L/mg) and K_F ($\text{mg}^{1-n} \text{L}^n/\text{g}$) are the Langmuir and Freundlich constants, respectively, and n is the Freundlich adsorption exponent.

Moreover, the Dubinin–Radushkevich (D–R) isotherm is applied to estimate the U(VI) adsorption behaviour (chemical or physical) onto the sorbent. The D–R equation⁶⁷ is written as follow:

Sorbents	pH	c/V (g/L)	Q _m (mg/g)
Tea wastes ⁴³	4	1.2	29.41
Tea waste ⁴⁵	6	0.2	142.21
Pyrolyzed tea wastes ⁴⁶	3	—	59.50
Green tea ⁶⁹	4~6	5	8.12
Tea waste ⁷⁰	6	—	43.19
Black tea scrap ⁷¹	5	4	62.51
TW (This work) ^{70,71}	5	0.5	91.72
GOTW (This work)	5	0.5	111.61
rGO/Fe ₃ O ₄ /TW (This work)	5	0.5	104.95

Table 4. Comparison of Q_m of as-obtained adsorbents in this study with the reported tea wastes for U(VI) adsorption.

Sorbents	ΔH ⁰ (kJ/mol)	ΔS ⁰ (J/(mol·k))	ΔG ⁰ (kJ/mol)			
			303 K	313 K	323 K	333 K
TW	45.24	183.91	-10.48	-12.32	-14.16	-16.00
GOTW	26.71	123.16	-10.61	-11.83	-13.07	-14.30
rGO/Fe ₃ O ₄ /TW	21.31	106.83	-11.06	-12.13	-13.20	-14.26

Table 5. Thermodynamic parameters of U(VI) adsorption on TW, GOTW and rGO/Fe₃O₄/TW.

$$\ln Q_e = \ln Q_m - \beta \varepsilon^2 \quad (9)$$

$$\varepsilon = RT \ln \left(1 + \frac{1}{C_e} \right) \quad (10)$$

where β (mol²/J²) is activity coefficient depending on the mean free energy of adsorption and ε is the Polanyi potential (J/mol). R and T represent the gas constant (8.314 J/mol K) and absolute temperature (K), respectively.

The D–R isotherm fit parameters of GO, TW, GOTW and rGO/Fe₃O₄/TW at different temperature are listed in Table 3. The D–R isotherm usually used the mean free energy E (kJ/mol) to assess the type of adsorption mechanism. The E value can be calculated according to Eq. (11). A value higher than 8 kJ/mol is considered to indicate chemical adsorption while it is less than 8 kJ/mol for the physical adsorption⁶⁸. Seen from Table 3, the calculated E value of GO, TW, GOTW and rGO/Fe₃O₄/TW at 289 K was 2.236 kJ/mol, 2.236 kJ/mol, 2.887 kJ/mol and 3.162 kJ/mol, respectively which indicated that physical adsorption occurs for U(VI) onto GO, TW, GOTW and rGO/Fe₃O₄/TW.

$$E = \frac{1}{\sqrt{2\beta}} \quad (11)$$

A comparison of the Q_m of different adsorbents is presented in Table 4. Table 4 shows that the Q_m of the prepared rGO/Fe₃O₄/TW indicated a promising adsorbent for the treatment of uranium-bearing wastewater.

Effect of temperature and adsorption thermodynamics. The enthalpy (ΔH⁰), entropy (ΔS⁰) and standard free energy ΔG⁰ from 303 K to 333 K in the adsorption process were calculated from the slope and intercept of the linear line of lnK_d versus 1/T using Eqs (12)~(14)¹⁵. The thermodynamic parameters and the plots of lnK_d versus 1/T onto TW, GOTW and rGO/Fe₃O₄/TW are shown in Table 5 and Fig. 10, respectively. The negative value of ΔH⁰ indicated that the adsorption reaction was endothermic. The positive ΔS⁰ and negative ΔG⁰ suggests that the adsorption process was spontaneous.

$$K_d = \frac{c_{ad}}{c_e} \quad (12)$$

$$\ln K_d = -\frac{\Delta H^0}{RT} + \frac{\Delta S^0}{R} \quad (13)$$

$$\Delta G^0 = \Delta H^0 - T\Delta S^0 \quad (14)$$

where K_d (mL/g) is the distribution coefficient of U(VI), c_{ad} (mg/L) is the concentration of metal ions on the adsorbent at equilibrium, c_e (mg/L) is the equilibrium concentration of metal ions in solution.

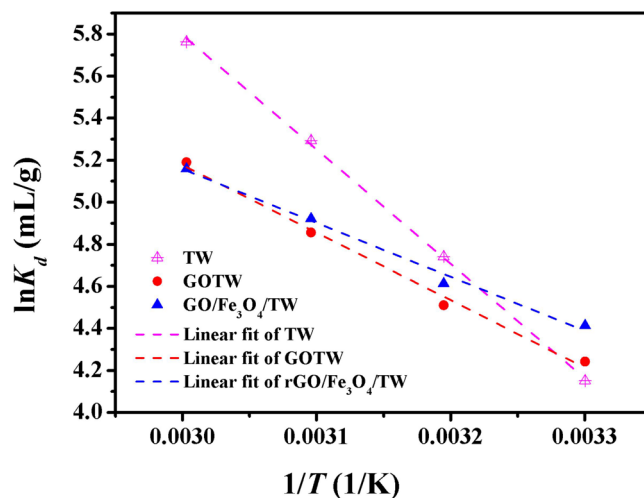


Figure 10. Plots of $\ln K_d$ versus $1/T$ for U(VI) adsorption onto TW, GOTW and rGO/Fe₃O₄/TW. pH = 5.0, $C_{(U)initial} = 10$ mg/L, $C_{sorbent} = 0.5$ g/L, $T = 303$ K, 313 K, 323 K and 333 K, and contact time = 24 h.

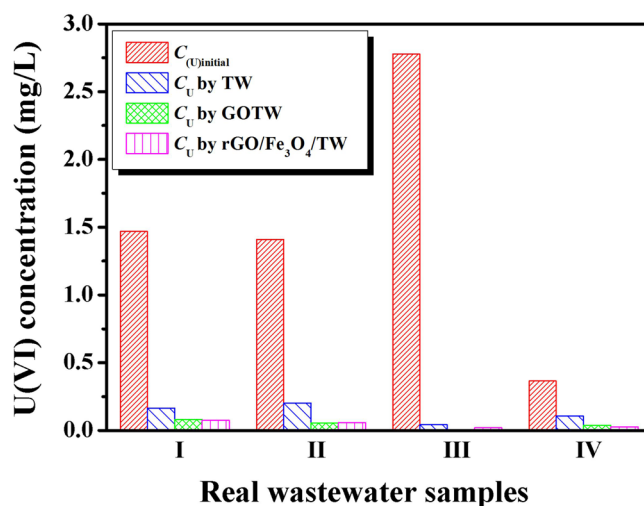


Figure 11. Column chart of adsorption efficiency of TW, GOTW and rGO/Fe₃O₄/TW for real uranium-bearing nuclear waste effluents. pH = 5.0, $C_{sorbent} = 0.5$ g/L, contact time = 1 h, and $T = 298$ K.

Wastewater parameters	Measured parameter values	Wastewater parameters	Measured parameter values
pH	7.0~8.0	U	0.3~3.0 mg/L
Al	≤0.05 mg/L	Ca	0~5.00 mg/L
B	≤0.05 mg/L	Be	≤0.05 mg/L
Cu	0~0.04 mg/L	Fe	≤0.34 mg/L
Mn	0~0.04 mg/L	Mg	0~1.38 mg/L
Si	0~2.71 mg/L	Mo	≤0.05 mg/L
Ni	0~0.02 mg/L		

Table 6. Measured parameter values of real uranium-bearing wastewater samples.

Real wastewater sample analysis. To evaluate the applicability of the prepared adsorbents in this study for real uranium-bearing wastewater samples, the removal efficiency of U(VI) from four different batches of wastewater samples under the optimum adsorption conditions was investigated. The measured parameters of real nuclear wastewater and adsorption experiment results are presented in Table 6 and Fig. 11, respectively. As shown in Fig. 11, co-existing ions had no effect on the removal efficiency of GOTW and rGO/Fe₃O₄/TW for uranium, and they can be applied in the treatment of uranium-containing nuclear waste effluents as potential adsorbents.

Materials and Methods

Materials. Stock solutions of uranium (5–150 mg/L) were prepared by dissolving $\text{UO}_2(\text{NO}_3)_2 \cdot 6\text{H}_2\text{O}$ (Xi'an Dingtian Chemical Reagent Co.) in deionized water (DW) and acidifying with a small amount of concentrated HNO_3 . The green tea used in this work originated from Sichuan Pingwu in China. All reagents used were of analytical grade and were used without further purification. DW was used throughout the experiments.

Preparation of tea wastes (TW). Green tea was washed with DW several times to remove all dirt substances. It was then boiled in DW at 80 °C for 1 h to remove coloured and soluble components, and then washed with DW until virtually colourless. The obtained TW was dried in an oven at 100 °C for 24 h. Finally, the products were crushed to powder in a pulveriser⁷².

Preparation of the composite GOTW. GO was prepared from natural graphite by the modified Hummers method⁷³. GOTW was prepared using GO and TW under ultrasonic treatment. Briefly, the mixture of GO (0.5 g) and TW (0.5 g) was dispersed in 100 ml DW under ultrasonication for 3 h. The obtained GOTW was centrifuged and washed with DW and ethanol. Finally, GOTW was dried at 50 °C under vacuum.

Preparation of the magnetic composite rGO/Fe₃O₄/TW. The rGO/Fe₃O₄/TW composite was synthesized using a previously reported method⁷⁴. First, a mixture of GO (0.25 g) and TW (0.25 g) was dispersed in 100 ml DW under ultrasonic treatment for 3 h. Then, 25% dilute ammonia solution was added drop-wise to the solution until the pH reached 11. Then, 1.25 g of $\text{FeCl}_2 \cdot 4\text{H}_2\text{O}$ was added very slowly to the mixture with continuous magnetic stirring. After stirring for 3 h, black rGO/Fe₃O₄/TW product was obtained by filtration and washed with DW and ethanol. Finally, rGO/Fe₃O₄/TW was dried at 50 °C under vacuum.

Characterization of the products. Fourier transform infrared (FTIR) spectra of as-prepared adsorbents were obtained using an FTIR spectrometer (Bruker VERTEX 70, Germany). The crystal phases of the samples were characterized by X-ray diffractometer (XRD) (2700 model, China). The surface morphology of the products was determined using a scanning electron microscope (SEM; FEI Helios 600i, USA). The magnetic measurements of Fe₃O₄ and rGO/Fe₃O₄/TW were conducted at 300 k under a varying magnetic field (PPMS-9 ECII, USA Quantum Design Co.). X-ray photoelectron spectroscopy (XPS) was studied using an ESCALAB 250 X-ray photoelectron spectroscopy (Thermo fisher, USA).

Adsorption experiments. The influence of pH, contact time, initial uranium concentration, and temperature on the removal efficiency of uranium were investigated. The solution pH was adjusted using NaOH and HCl. The prepared adsorbent was added to 20 mL U(VI) solution and shaken in a shaker (Kangshi, China). After filtration, residual uranium concentrations were measured by a micro-quantity uranium analyser (MUA model, China). The removal rate R (%) and the adsorption capacity of U(VI) Q (mg/g) were calculated according to Eqs (15) and (16), respectively:

$$R(\%) = \frac{c_0 - c_t}{c_0} \times 100 \quad (15)$$

$$Q(\text{mg/g}) = \frac{(c_0 - c_t)}{W} \times V \quad (16)$$

where c_0 (mg/L) is the initial uranium (VI) concentration, c_t (mg/L) is the uranium concentration at time t , V (L) is the solution volume and W (g) stands for the weight of adsorbent.

Conclusion

In summary, four adsorbents GO, TW, GOTW and rGO/Fe₃O₄/TW were fabricated for the adsorption of uranium from aqueous solutions. The adsorption data of U(VI) by TW, GOTW and rGO/Fe₃O₄/TW were consistent with the Langmuir isotherm model and pseudo-second-order kinetics. The composites GOTW and rGO/Fe₃O₄/TW exhibited higher adsorption capacities and faster adsorption kinetics than did GO and TW. The results showed that GOTW and rGO/Fe₃O₄/TW could be utilized effectively as promising sorbents to removal uranium from real multi-component uranium-containing nuclear waste effluents. Furthermore, due to the advantageous magnetic properties, rGO/Fe₃O₄/TW can be easily separated from aqueous solutions, thus enhancing post-treatment efficiency for further practical applications.

References

1. Skinner, L. B. *et al.* Molten uranium dioxide structure and dynamics. *Science* **346**(6212), 984–987 (2014).
2. Yu, J., Wang, J.-L. & Jiang, Y.-Z. Removal of uranium from aqueous solution by alginate beads. *Nuclear Engineering and Technology*. **49**(3), 534–540 (2017).
3. El-Maghrabi, H. H. *et al.* Magnetic graphene based nanocomposite for uranium scavenging. *Journal of Hazardous Materials*. **322**(Part B), 370–379 (2017).
4. Torkabad, M. G., Keshtkar, A. R. & Safdari, S. J. Comparison of polyethersulfone and polyamide nanofiltration membranes for uranium removal from aqueous solution. *Progress in Nuclear Energy*. **94**, 93–100 (2017).
5. Torkabad, M. G., Keshtkar, A. R. & Safdari, S. J. Uranium membrane separation from binary aqueous solutions of UO_2^{2+} - K^+ and UO_2^{2+} - Ca^{2+} by the nanofiltration process. *Separation Science and Technology*. **52**(6), 1095–1105 (2017).
6. He, H.-C. *et al.* Simultaneous removal and recovery of uranium from aqueous solution using TiO₂ photoelectrochemical reduction method. *Journal of Radioanalytical and Nuclear Chemistry*. **313**(1), 59–67 (2017).
7. Xu, J. *et al.* Efficacy of acetate-amended biostimulation for uranium sequestration: Combined analysis of sediment/groundwater geochemistry and bacterial community structure. *Applied Geochemistry*. **78**, 172–185 (2017).

8. Kim, G. N. *et al.* Remediation of soil/concrete contaminated with uranium and radium by biological method. *Journal of Radioanalytical and Nuclear Chemistry*. **297**(1), 71–78 (2013).
9. Beltrami, D. *et al.* Recovery of uranium from wet phosphoric acid by solvent extraction processes. *Chemical Reviews*. **114**, 12002–12023 (2014).
10. Chen, M.-M. *et al.* The extraction of uranium using graphene aerogel loading organic solution. *Talanta*. **166**, 284–291 (2017).
11. Ogden, M. D. *et al.* Application of chelating weak base resin Dowex M4195 to the recovery of uranium from mixed sulfate/chloride media. *Chemical Engineering Journal*. **317**, 80–89 (2017).
12. Li, J.-Q. *et al.* Direct extraction of U(VI) from alkaline solution and seawater via anion exchange by metal-organic framework. *Chemical Engineering Journal*. **316**, 154–159 (2017).
13. Li, W. *et al.* Versatile inorganic–organic hybrid WO_x-ethylenediamine nanowires: Synthesis, mechanism and application in heavy metal ion adsorption and catalysis. *Nano Research*. **7**(6), 903–916 (2014).
14. Budnyak, T. M. *et al.* Silica with immobilized phosphinic acid-derivative for uranium extraction. *Journal of Hazardous Materials*. **314**(1), 326–340 (2016).
15. Abdi, S. *et al.* Investigation of uranium (VI) adsorption by polypyrrole. *Journal of Hazardous Materials*. **332**(1), 132–139 (2017).
16. Pan, D.-Q. *et al.* Removal of uranium contaminant from aqueous solution by chitosan@attapulgite composite. *Separation and Purification Technology*. **177**, 86–93 (2017).
17. El-Bohy, M. N. *et al.* Grafting of arginine and glutamic acid onto cellulose for enhanced uranyl sorption. *Cellulose*. **24**(3), 1427–1443 (2017).
18. Guo, X. *et al.* Phosphoryl functionalized mesoporous silica for uranium adsorption. *Applied Surface Science*. **402**, 53–60 (2017).
19. Elshehy, E. A. Removal of uranium ions from liquid radioactive waste using modified aluminosilica. *Separation Science and Technology*. **52**(11), 1852–1861 (2017).
20. Wang, Z.-S. *et al.* Improving the adsorption ability of graphene sheets to uranium through chemical oxidation, electrolysis and ball-milling. *Journal of Radioanalytical and Nuclear Chemistry*. **308**(3), 1095–1102 (2017).
21. Tran, D. Q., Pham, H. T. & Do, H. Q. Efficient Removal of uranium from aqueous solution by reduced graphene oxide–Zn_{0.5}Ni_{0.5}Fe₂O₄ ferrite–polyaniline nanocomposite. *Journal of Electronic Materials*. **46**(6), 3273–3278 (2017).
22. Decker, J. D. *et al.* Ship-in-a-bottle CMPO in MIL-101(Cr) for selective uranium recovery from aqueous streams through adsorption. *Journal of Hazardous Materials*. **335**(1), 1–9 (2017).
23. Liu, S.-J. *et al.* Adsorption equilibrium and kinetics of uranium onto porous azo-metal–organic frameworks. *Journal of Radioanalytical and Nuclear Chemistry*. **310**(1), 353–362 (2016).
24. Naeem, H. *et al.* Uranium remediation using modified Vigna radiata waste biomass. *Applied Radiation and Isotopes*. **123**(1), 94–101 (2017).
25. Yi, Z.-J. *et al.* Biosorption characteristics of ceratophyllum demersum biomass for removal of uranium(VI) from an aqueous solution. *Journal of Radioanalytical and Nuclear Chemistry*. **313**(1), 19–27 (2017).
26. Yakout, S. M. & Rizk, M. A. Adsorption of uranium by low-cost adsorbent derived from agricultural wastes in multi-component system. *Desalination and Water Treatment*. **53**(7), 1917–1922 (2015).
27. Mahmoud, G. A. A novel hydrogel based on agricultural waste for removal of hazardous dyes from aqueous solution and reuse process in a secondary adsorption. *Polymer Bulletin*. **74**(2), 337–358 (2017).
28. Yu, F. *et al.* Biosorbents based on agricultural wastes for ionic liquid removal: An approach to agricultural wastes management. *Chemosphere*. **165**(1), 94–99 (2016).
29. Caccin, M. *et al.* Adsorption of uranium, cesium and strontium onto coconut shell activated carbon. *Journal of Radioanalytical and Nuclear Chemistry*. **297**(1), 9–18 (2013).
30. Ramarajan, R. & Manohar, C. S. Biological pretreatment and bioconversion of agricultural wastes, using ligninolytic and cellulolytic fungal consortia. *Bioremediation Journal*. **21**(2), 89–99 (2017).
31. Gómez-Mascaraque, L. G., Hernández-Rojas, M. & Tarancón, P. *et al.* Impact of microencapsulation within electrosprayed proteins on the formulation of green tea extract-enriched biscuits. *LWT-Food Science and Technology*. **81**, 77–86 (2017).
32. Johnson, R., Bryant, S. & Huntley, A. L. Green tea and green tea catechin extracts: an overview of the clinical evidence. *Maturitas*. **73**, 280–287 (2012).
33. Dieng, H. R. *et al.* Green tea and its waste attract workers of formicine ants and kill their workers—implications for pest management. *Industrial Crops and Products*. **89**, 157–166 (2016).
34. Peng, C.-Y. *et al.* Highly selective defluoridation of brick tea infusion by tea waste supported aluminum oxides. *Journal of the Science of Food and Agriculture*. **97**(5), 1509–1516 (2017).
35. Foroughi-dahr, M., Abolghasemi, H. & Esmaili, M. *et al.* Experimental study on the adsorptive behavior of Congo red in cationic surfactant-modified tea waste. *Process Safety and Environmental Protection*. **95**(1), 226–236 (2015).
36. Kan, Y.-J., Yue, Q.-Y. & Li, D. *et al.* Preparation and characterization of activated carbons from waste tea by H₃PO₄ activation in different atmospheres for oxytetracycline removal. *Journal of the Taiwan Institute of Chemical Engineers*. **71**(Complete), 494–500 (2017).
37. Tzeng, J.-H., Weng, C.-H. & Huang, J.-W. *et al.* Spent tea leaves: A new non-conventional and low-cost biosorbent for ethylene removal. *International Biodeterioration & Biodegradation*. **104**(1), 67–73 (2015).
38. Yang, S.-X., Wu, Y.-H. & Aierken, A. *et al.* Mono/competitive adsorption of Arsenic(III) and Nickel(II) using modified green tea waste. *Journal of the Taiwan Institute of Chemical Engineers*. **60**(1), 213–221 (2016).
39. Weng, C.-H., Lin, Y.-T. & Hong, D.-Y. *et al.* Effective removal of copper ions from aqueous solution using base treated black tea waste. *Ecological Engineering*. **67**(6), 127–133 (2014).
40. Gupta, A. & Balomajumder, C. Simultaneous adsorption of Cr(VI) and phenol onto tea waste biomass from binary mixture: Multicomponent adsorption, thermodynamic and kinetic study. *Journal of Environmental Chemical Engineering*. **3**(2), 785–796 (2015).
41. Yang, X.-P. & Cui, X.-N. Adsorption characteristics of Pb(II) on alkali treated tea residue. *Water Resources and Industry*. **3**(Complete), 1–10 (2013).
42. Shen, B.-X., Tian, L.-H. & Li, F.-K. *et al.* Elemental mercury removal by the modified bio-char from waste tea. *Fuel*. **187**(Complete), 189–196 (2017).
43. Li, X.-Y., Li, F.-B. & Jin, Y. *et al.* The uptake of uranium by tea wastes investigated by batch, spectroscopic and modeling techniques. *Journal of Molecular Liquids*. **209**(1), 413–418 (2015).
44. Khajeh, M., Bohlooli, M. & Jahanbin, E. *et al.* Box-Behnken design in modeling of solid-phase tea waste extraction for the removal of uranium from water samples. *Radiochimica Acta*. **103**(5), 379–384 (2015).
45. Ding, D.-X., Liu, X.-T. & Hu, N. *et al.* Removal and recovery of uranium from aqueous solution by tea waste. *Journal of Radioanalytical and Nuclear Chemistry*. **293**(3), 735–741 (2012).
46. Aly, Z. & Luca, V. Uranium extraction from aqueous solution using dried and pyrolyzed tea and coffee wastes. *Journal of Radioanalytical and Nuclear Chemistry*. **295**(1), 889–900 (2013).
47. Tang, J. & Yamauchi, Y. Carbon materials: MOF morphologies in control. *Nature Chemistry*. **8**(7), 638–639 (2016).
48. Yoon, Y., Zheng, M.-L. & Ahn, Y.-T. *et al.* Synthesis of magnetite/non-oxidative graphene composites and their application for arsenic removal. *Separation and Purification Technology*. **178**(Complete), 40–48 (2017).
49. Hu, B.-W., Hu, Q.-Y. & Li, X. *et al.* Rapid and highly efficient removal of Eu(III) from aqueous solutions using graphene oxide. *Journal of Molecular Liquids*. **229**(Complete), 6–14 (2017).
50. Ansari, M. O., Kumar, R. & Ansari, S. A. *et al.* Anion selective pTSA doped polyaniline@graphene oxide-multiwalled carbon nanotube composite for Cr(VI) and Congo red adsorption. *Journal of Colloid and Interface Science*. **496**(Complete), 407–415 (2017).

51. Mohan, S., Kumar, V. & Singh, D. K. *et al.* Effective removal of lead ions using graphene oxide-MgO nanohybrid from aqueous solution: Isotherm, kinetic and thermodynamic modeling of adsorption. *Journal of Environmental Chemical Engineering* **5**(3), 2259–2273 (2017).
52. Tan, P., Bi, Q. & Hu, Y.-Y. *et al.* Effect of the degree of oxidation and defects of graphene oxide on adsorption of Cu²⁺ from aqueous solution. *Applied Surface Science* **423**(1), 1141–1151 (2017).
53. Wang, X., Liu, Q. & Liu, J.-Y. *et al.* 3D self-assembly polyethyleneimine modified graphene oxide hydrogel for the extraction of uranium from aqueous solution. *Applied Surface Science* **426**(1), 1063–1074 (2017).
54. Georgakilas, V., Tiwari, J. N. & Kemp, K. C. *et al.* Noncovalent functionalization of graphene and graphene oxide for energy materials, biosensing, catalytic, and biomedical applications. *Chemical Reviews* **116**(9), 5464–5519 (2016).
55. Zhou, R.-S., Zhou, R.-W. & Zhang, X.-H. *et al.* An efficient bio-adsorbent for the removal of dye: Adsorption studies and cold atmospheric plasma regeneration. *Journal of the Taiwan Institute of Chemical Engineers* **68**(1), 372–378 (2016).
56. Pan, N., Li, L. & Ding, J. *et al.* Preparation of graphene oxide-manganese dioxide for highly efficient adsorption and separation of Th(IV)/U(VI). *Journal of Hazardous Materials* **309**(1), 107–115 (2016).
57. Atarod, M., Nasrollahzadeh, M. & Sajadi, S. M. Green synthesis of Pd/RGO/Fe₃O₄ nanocomposite using Withania coagulans leaf extract and its application as magnetically separable and reusable catalyst for the reduction of 4-nitrophenol. *Journal of Colloid and Interface Science* **465**(1), 249–258 (2016).
58. Madhuvilakku, R., Alagar, S. & Mariappan, R. *et al.* Green one-pot synthesis of flowers-like Fe₃O₄/rGO hybrid nanocomposites for effective electrochemical detection of riboflavin and low-cost supercapacitor applications. *Sensors and Actuators B* **253**(1), 879–892 (2017).
59. Cai, H.-M., Chen, G.-J. & Peng, C.-Y. *et al.* Removal of fluoride from drinking water using tea waste loaded with Al/Fe oxides: A novel, safe and efficient biosorbent. *Applied Surface Science* **328**(1), 34–44 (2015).
60. Wu, Y., Luo, H.-J. & Wang, H. *et al.* Fast adsorption of nickel ions by porous graphene oxide/sawdust composite and reuse for phenol degradation from aqueous solutions. *J. Colloid. Interf. Sci.* **436**(Complete), 90–98 (2014).
61. Chen, S., Hong, J. & Yang, H. *et al.* Adsorption of uranium (VI) from aqueous solution using a novel graphene oxide-activated carbon felt composite. *Journal of Environmental Radioactivity* **126**(Complete), 253–258 (2013).
62. Liu, X.-H., Cheng, C. & Xiao, C.-J. *et al.* Polyaniline (PANI) modified bentonite by plasma technique for U(VI) removal from aqueous solution. *Applied Surface Science* **411**(1), 331–337 (2017).
63. Lagergren, S. Zur theorie der sogenannten adsorption gelöster stoffe. *Kungliga. Svenska Vetensk. Handl* **24**, 1–39 (1898).
64. Ho, Y. & McKay, G. Pseudo-second order model for sorption processes. *Process Biochem.* **34**(5), 451–465 (1999).
65. Vu, H.-C., Dwivedi, A.-D. & Le, T.-T. *et al.* Magnetite graphene oxide encapsulated in alginate beads for enhanced adsorption of Cr(VI) and As(V) from aqueous solutions: Role of crosslinking metal cations in pH control. *Chemical Engineering Journal* **307**(Complete), 220–229 (2017).
66. Shao, L., Wang, X.-F. & Ren, Y.-M. *et al.* Facile fabrication of magnetic cucurbit[6]uril/graphene oxide composite and application for uranium removal. *Chemical Engineering Journal* **286**(1), 311–319 (2016).
67. Saleh, T. A., Sari, A. & Tuzen, M. Effective adsorption of antimony(III) from aqueous solutions by polyamide-graphene composite as a novel adsorbent. *Chemical Engineering Journal* **307**, 230–238 (2017).
68. Yen, C.-H., Lien, H.-L., Chung, J.-S. & Yeh, H.-D. Adsorption of precious metals in water by dendrimer modified magnetic nanoparticles. *Journal of Hazardous Materials* **322**, 215–222 (2017).
69. Zhou, F. L., Xie, X. F. & Tang, H. *et al.* Adsorption behavior of uranium ion and thorium ion on green tea. *Chinese Journal of Analytical Chemistry* **30**(3), 355–358 (2002).
70. Liu, X. T., Li, G. Y. & Hu, N. *et al.* Adsorption characteristics of U(VI) on tea waste. *CIESC. Journal.* **63**(10), 3291–3296 (2012).
71. Chen, A. S., Zhang, H. & Chen, D. Q. *et al.* Adsorption properties for uranyl ion by black tea scrap. *Hydrometallurgy of China* **33**(2), 128–132 (2014).
72. Madrakian, T., Afkhami, A. & Ahmadi, M. Adsorption and kinetic studies of seven different organic dyes onto magnetite nanoparticles loaded tea waste and removal of them from wastewater samples. *Spectrochimica Acta Part A: Molecular and Biomolecular Spectroscopy* **99**(Complete), 102–109 (2012).
73. Ma, J., Liu, C.-H. & Li, R. *et al.* Properties and structural characterization of oxide starch/chitosan/graphene oxide biodegradable nanocomposites. *Journal of Applied Polymer Science* **123**(5), 2933–2944 (2012).
74. Boruah, P. K., Borah, D. J. & Handique, J. *et al.* Facile synthesis and characterization of Fe₃O₄ nanopowder and Fe₃O₄/reduced graphene oxide nanocomposite for methyl blue adsorption: A comparative study. *Journal of Environmental Chemical Engineering* **3**(3), 1974–1985 (2015).

Acknowledgements

This work was supported by the National Natural Science Foundation of China (No. 21407132). We also gratefully acknowledge Xiandong Meng, Qifa Pan and Yi Liu for the characterization of the samples.

Author Contributions

Author contributions were as follows: Aili Yang designed the research. Aili Yang, Yukuan Zhu and Ping Li performed the experiments. Aili Yang analyzed the data and wrote the paper. C.P. Huang guided the experiments and revised the paper.

Additional Information

Competing Interests: The authors declare no competing interests.

Publisher's note: Springer Nature remains neutral with regard to jurisdictional claims in published maps and institutional affiliations.



Open Access This article is licensed under a Creative Commons Attribution 4.0 International License, which permits use, sharing, adaptation, distribution and reproduction in any medium or format, as long as you give appropriate credit to the original author(s) and the source, provide a link to the Creative Commons license, and indicate if changes were made. The images or other third party material in this article are included in the article's Creative Commons license, unless indicated otherwise in a credit line to the material. If material is not included in the article's Creative Commons license and your intended use is not permitted by statutory regulation or exceeds the permitted use, you will need to obtain permission directly from the copyright holder. To view a copy of this license, visit <http://creativecommons.org/licenses/by/4.0/>.

© The Author(s) 2019